Fragmentation of stable and neutron-rich $^{12-16}$C into boron fragments at approximately 240 MeV/nucleon*

Shu-Ya Jin(金树亚)[1,2,3] Ya-Zhou Sun(孙亚洲)[4] Shi-Tao Wang(王世陶)[1,2†] Zhi-Yu Sun(孙志宇)[1,2]
Xue-Heng Zhang(章学恒)[1,2] Zhi-Qiang Chen(陈志强)[1,2] Bo Mei(梅波)[5] Yi-Xuan Zhao(赵亦轩)[1,2,3]
Shu-Wen Tang(唐述文)[1,2] Yu-Hong Yu(余玉洪)[1,2] Duo Yan(闫铎)[1] Fang Fang(方芳)[1]
Yong-Jie Zhang(张永杰)[1] Shao-bo Ma(马少波)[1] Xiang-Man Liu(刘相满)[1] Rui Han(韩瑞)[1]

[1]CAS Key Laboratory of High Precision Nuclear Spectroscopy, Institute of Modern Physics, Chinese Academy of Sciences, Lanzhou 730000, China
[2]School of Nuclear Science and Technology, University of Chinese Academy of Sciences, Beijing 100080, China
[3]School of Nuclear Science and Technology, Lanzhou University, Lanzhou 730000, China
[4]School of Physics and Electrical Engineering, Anyang Normal University, Anyang 455000, China
[5]Sino-French Institute of Nuclear Engineering and Technology, Sun Yat-sen University, Zhuhai 519082, China

Abstract: The elemental fragmentation cross sections of boron fragments produced by stable and neutron-rich $^{12-16}$C beams with a carbon target were systematically measured at an incident beam energy of approximately 240 MeV/nucleon. The measured cross sections were found to increase as the projectile mass number increases. The observed feature is explained qualitatively based on the abrasion-ablation two-stage reaction model and is compared quantitatively with predictions from various reaction models, including empirical and statistical models. All models agree with the measured cross sections within a factor of 2.

Keywords: elemental fragmentation cross sections, neutron-rich carbon isotopes, abrasion-ablation model

DOI: 10.1088/1674-1137/ac2ed5

I. INTRODUCTION

For decades, radioactive ion beams have been extensively used for the study of exotic nuclei [1–8]. One of the most widely used methods of producing radioactive ion beams is based on projectile fragmentation reactions and the in-flight separation technique. Recently, fragmentation reactions with unstable projectiles were investigated to produce extremely neutron-rich nuclei [9]. Fragmentation reactions with stable and unstable projectiles have an important impact on various research fields, such as heavy-ion cancer therapy [10, 11] and radiation protection [12]. When designing experiments, reliable fragmentation reaction models are required to accurately predict the yield of fragments produced from stable or unstable beams. The statistical abrasion-ablation model [13], intranuclear-cascade approach [14], and empirical models, such as EPAX [15], FRACS [16], and NUCFRG [17] are widely used to predict fragmentation cross sections. However, most of the existing experimental data are obtained from the fragmentation of stable nuclei, and the empirical models are developed by mainly relying on stable nuclear fragmentation data. Systematic fragmentation data, including radioactive isotopes within a long isotopic chain, are still scarce; thus, systematic measurements of radioactive nuclear fragmentation cross sections can expand the relevant nuclear interaction cross sections database and test and further develop reaction models.

Elemental fragmentation cross sections and individual isotopic fragmentation cross sections of the stable ^{12}C beams have been extensively measured on different targets and in various energy regions [18–20]. Fragmentation of carbon isotopes not only provides information for understanding the reaction mechanism, but is also relevant to applied physics, such as carbon therapy and space radiation protection; for example, ^{12}C beams is widely used in radiotherapy [21, 22]. In addition, unstable carbon beams have recently been proposed for radiotherapy [23]. However, information on the elemental fragmentation cross sections of unstable carbon beams is incomplete.

In this paper, we report on a systematic measurement of boron elemental fragment production cross sections

Received 13 July 2021; Accepted 12 October 2021; Published online 4 November 2021

* Supported by the National Natural Science Foundation of China (U1732134, U1832205), the Heavy Ion Research Facility in Lanzhou (HIRFL), and the open research project of CAS large research infrastructures

† E-mail: wangshitao@impcas.ac.cn

from neutron-rich $^{14-16}$C and stable ^{12,13}C beams impinging on a carbon target at beam energies of approximately 240 MeV/nucleon. Our aim is to investigate the dependence of fragmentation cross sections on the isospin of a projectile, which can improve our understanding of the mechanism behind the fragmentation process.

II. EXPERIMENT

Experiments were performed at the Heavy Ion Research Facility (HIRFL) [24–27] of the Institute of Modern Physics, Chinese Academy of Sciences. An ^{18}O primary beam with an intensity of $\approx 10^6$ particles per second was accelerated to 280 MeV/nucleon by the main Cooler Storage Ring (CSRm) synchrotron and impinged on a 15-mm-thick ^{9}Be production target. The secondary cocktail beams of interest produced by the projectile fragmentation of ^{18}O were separated and identified by the Second Radioactive Ion Beam Line in Lanzhou (RIBLL2) [28] and delivered to the External Target Facility (ETF) [29] area for the experiments. Fig. 1 presents a schematic diagram of the layout of the RIBLL2 and the employed detectors at the ETF terminal. Five magnetic field settings were applied to the RIBLL2 to produce the $^{12-16}$C secondary beams. The particle identification for the secondary beams is achieved based on the measurements of time-of-flight (TOF) and energy loss (ΔE). The TOF was measured between two plastic scintillator detectors separated by 26 m and denoted by SC0 and SC1 [30] in Fig. 1. The energy loss was measured using a multiple sampling ionization chamber (denoted by MUSIC0). A typical particle identification spectrum for the ^{16}C setting is shown in Fig. 2, which reveals a clean separation between the different constituents of the secondary beams. A typical value for the secondary beam intensity is 100 particles per second.

The secondary beams impinged on a 900-mg/cm^2-thick carbon reaction target with a diameter of 50 mm to induce the fragmentation reaction. Average center-of-target energies were approximately 240 MeV/nucleon for the $^{12-16}$C secondary beams. Two multi-wire drift chambers (MWDC0 and MWDC1), located upstream of the carbon target and each with an active area of 13×13 cm^2, were used to measure the trajectories of the incoming particles and restrict the beam spot on the target in the off-line analysis.

Downstream of the carbon target, the trajectories of the outgoing particles are monitored by MWDC2 and MWDC3 with the same active area as those upstream of the target. A multiple sampling ionization chamber [31] (MUSIC1) with an active area of 13×13 cm^2 was used to identify the charges of the outgoing particles. The energy loss information, measured by MUSIC1, was converted into the charge number Z of the outgoing particles by applying the relation $\Delta E \sim Z^2/v^2$, where the velocity v was assumed to be constant. A clear charge number Z separation was obtained for the carbon and boron isotopes, as shown in Fig. 3, for the ^{16}C beam setting. The achieved resolution is approximately 0.24 and 0.41 charge units (full width at half maximum) for the carbon and boron isotopes, respectively. The Z resolution descreases as the number of lost charges increases. For events with one or more protons removed from the projectiles, it is possible that the large-acceptance MUSIC1 detector captured several charged fragments. The multitude of possible charged fragment combinations results in overlapping ΔE distributions; thus, the Z resolution deteriorates. In addition, the thickness of the secondary carbon target cannot be ignored. As a result, fragments generated at the entrance or exit of the target will have different energy losses in the target and therefore different outgoing velocities. Because the energy loss depends not only on the charge Z but also on the velocity, the width of the outgoing velocity distribution will deteriorate the Z resolution.

Measurements without the target were also performed with the same beam conditions as the target-in runs. The results are used to estimate the interaction probability in the detector setup and the air gap between detectors. As shown in Fig. 3, the interaction probability in the target-out runs is small compared to that with the target. In the off-line analysis, to avoid the influence of the reaction on the target frame, the size of the beam spot on the target was limited to 4 cm in diameter by installing a software gate using the position information provided by the MWDCs in front of the target. The sensitive area of the MUSIC1 detector is sufficiently large to cover almost

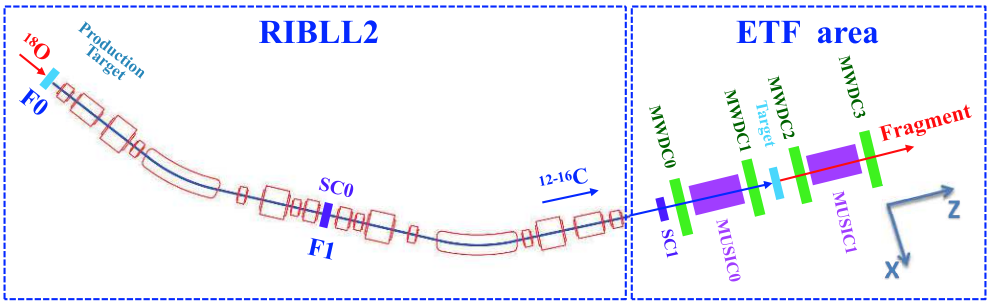

Fig. 1. (color online) Schematic view of the layout of the RIBLL2 and the detectors at the ETF area.

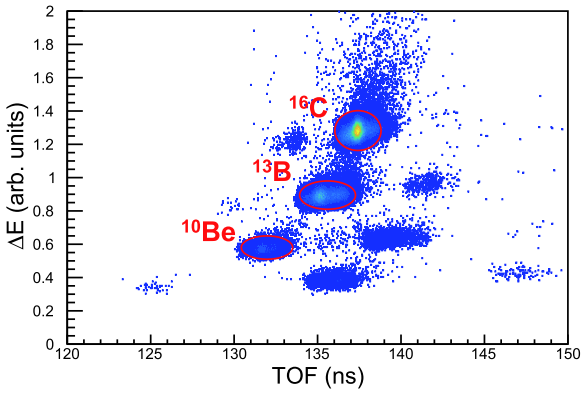

Fig. 2. (color online) A typical particle identification spectrum of the secondary beams for the ^{16}C setting.

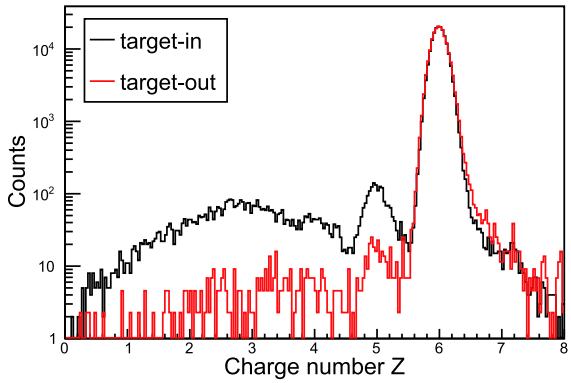

Fig. 3. (color online) A typical charge number Z identification spectrum for the ^{16}C beam. The black and red lines represent the target-in and the target-out run data, respectively. The target-out run result is multiplied by a factor of 2.28 to compare with the target-in run result.

the all outgoing boron particles, as shown in Fig. 4.

The elemental fragmentation cross sections σ are obtained from

$$\sigma = \frac{1}{t}\frac{N_o}{N_i}, \tag{1}$$

where t represents the number of atoms in the carbon target per unit area. N_i and N_o denote the number of incoming carbon projectiles and outgoing boron fragments, respectively, corrected by the target-out runs. The number of incoming projectiles, N_i, is determined by creating a 3σ ellipse gate on the ΔE-TOF two-dimensional particle identification spectrum. The number of outgoing fragments, N_o, is obtained by integrating the reaction residue peak area within 3σ in the charge number Z spectrum. The obtained elemental fragmentation cross sections of the boron fragments from beams of the carbon isotopes $^{12-16}$C are $\sigma(^{16}\text{C}\rightarrow\text{B}) = 189(9)$ mb, $\sigma(^{15}\text{C}\rightarrow\text{B}) = 176(10)$ mb, $\sigma(^{14}\text{C}\rightarrow\text{B}) = 160(9)$ mb, $\sigma(^{13}\text{C}\rightarrow\text{B}) = 127(13)$ mb, and $\sigma(^{12}\text{C}\rightarrow\text{B}) = 119(13)$ mb, as shown in

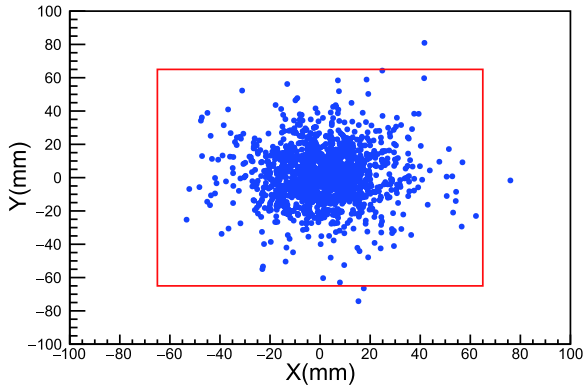

Fig. 4. (color online) Two-dimensional (X-Y) distribution spectrum of the outgoing boron particles on the MUSIC1 detector for the ^{16}C beam. The red rectangle denotes the sensitive area of MUSIC1.

Fig. 5. Besides the statistical error, the quoted uncertainty includes contributions from the background subtraction. For comparison, the reported cross sections for ^{12}C beams at similar incident energies are also shown in Fig. 5. Out measurement for ^{12}C projectiles is in good agreement with the reported values from Zeitlin *et al.* [32] and Kidd *et al.* [33]; however, the measured value by Ogawa *et al.* [34] is much lower than all other data.

III. DISCUSSION

A clear trend for the boron production cross sections along the carbon isotopic chain is observed in Fig. 5, where the cross sections increase with increasing neutron number of the carbon projectiles. This feature can be well understood in terms of the abrasion-ablation model [35].

First, a brief description of the abrasion-ablation model is presented. The abrasion-ablation model describes the fragmentation process using a two-step reaction scheme [36]. In the abrasion step, the overlapping zone of the projectile and target interact and nucleons abraded from the projectile only depend on the impact parameter. In this step, the neutron-to-proton ratio of the pre-fragments is related to the neutron-to-proton ratio of the projectile [35]. In the ablation step, the final fragmentation products are formed by de-exciting the pre-fragments through the evaporation of light particles [35]. The evaporation chain stops if the excitation energy of the pre-fragments decreases below the lowest particle-emission threshold energies. The neutron-to-proton ratio of the final projectile-like fragmentation products is related to the neutron-to-proton ratio of the projectile because the excitation energy of the pre-fragments obtained in the abrasion step is not sufficient to wash out the neutron excess in the evaporation process [37]. A statistical model was used to describe the evaporation probabilities of light particles; in the calculations, the abrasion-ablation model was implemented in the LISE++ code [38]. An average excitation

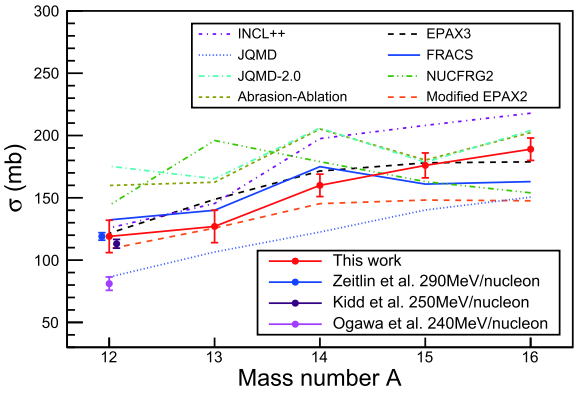

Fig. 5. (color online) Boron production cross sections versus mass number A of the incoming carbon isotopes impinging on the carbon target in this study (red line) and in literature data. The experimental cross sections are compared with EPAX3 (black line), Modified EPAX2 (orange line), FRACS (blue line), NUCFRG2 (green line), JQMD (light blue line), JQMD-2.0 (cyan line), INCL++ (magenta line), and the abrasion-ablation model (yellow line).

energy of 13.3 MeV per abraded nucleon, provided by the statistical hole-energy model [35], was adopted for the calculations.

The trend for the boron production cross sections along the carbon isotopic chain can be explained using the abrasion-ablation model. The production cross sections of boron isotopes receive contributions from two paths: (i) the removal of one proton and x ($x \geqslant 0$) neutrons in the first step, followed by the evaporation of y ($y \geqslant 0$) neutrons in the second step; and (ii) the removal of one or more neutrons in the first step, followed by the evaporation of one proton and z ($z \geqslant 0$) neutrons in the second step.

For path (i), because the proton distribution radii of $^{12-16}$C isotopes are very close [39], the probability of removing one proton from different carbon isotopes, irrespective of the number of removed neutrons, is approximately equal in the abrasion step. Along the carbon isotopic chain, the proton (neutron) separation energy increases (decreases) as the neutron-to-proton ratio increases. As a result, the nuclei with a large neutron excess will have a greater probability of evaporating neutrons instead of protons. Because there are similar boron pre-fragment production cross sections for different carbon isotopes in the abrasion stage and the suppression of proton evaporation increases with increasing neutron number in the projectiles, the boron fragment cross sections are expected to increase with increasing neutron number in the carbon projectiles. For path (ii), proton evaporation following neutron removal is expected to be negligible [39] for $^{12-16}$C because their proton separation energies are fairly large. Therefore, the boron production cross sections from the two paths are expected to increase as the projectile mass number increases; this is in agreement with the experimental results. As shown in Fig. 5, the growing trend of the experimental result is generally well reproduced by the abrasion-ablation model. In a previous study on the fragmentation of neutron-rich oxygen isotopes [40], the general behavior of the experimental cross sections of specific carbon, nitrogen, and oxygen fragments was also effectively described by the abrasion-ablation model.

To further probe the boron production cross sections along the carbon isotopic chain, the experimental data are compared with several other model calculations besides the abrasion-ablation model. Existing models that are used to predict reaction cross sections include statistical models and empirical parameterization. As these models are usually developed based on the fragmentation of stable nuclei, it is interesting to investigate their ability to predict the fragmentation cross sections of unstable nuclei. For this purpose, we compare the measured cross sections with predictions obtained from EPAX3, modified EPAX2, FRACS, NUCFRG2, JQMD, JQMD-2.0, and INCL++, which are widely used models for calculating fragmentation cross sections. The calculated results are shown in Fig. 5. In general, all models agree reasonably well with the measured cross sections within a factor of 2.

The EPAX parameterization is obtained by fitting the experimental data, which are mainly based on medium- to heavy-mass stable nuclei fragmentation [15, 41]. Therefore, the range of validity of the EPAX formula is $A > 40$ and the incident energy is above 64 MeV/nucleon [15]. Although the present data are outside the range limit for EPAX, the general data trend is well reproduced by EPAX. As EPAX parametrization is independent of the bombarding energy, a modified version of EPAX2, including the projectile energy dependence, was proposed by Zhang [42]. As shown in Fig. 5, the modified EPAX2 reproduces the general trend of experimental data.

FRACS is developed based on the EPAX parameterization and introduces several modifications to improve the predictive power for fragmentation cross sections [16]. The target and projectile energy dependencies, which are not included in EPAX, are considered in the FRACS parameterization. Furthermore, an additional term used to describe the odd-even staggering observed in many experiments is implemented in FRACS. The present data are generally well reproduced by FRACS. Nevertheless, the predicted trends from ^{14}C to ^{16}C are somewhat inconsistent with the observed results.

The NUCFRG2 model [17] is developed upon the abrasion-ablation model [43]. It is based on the fragmentation data of the proton beam and assumes that the nuclei are solid spheres with uniform nuclear matter distributions. As seen in Fig. 5, while the magnitude of the experimental cross sections is well reproduced overall, the predicted trend by the NUCFRG2 model deviates from the experimental data.

The Liège intranuclear cascade model (INCL++) [44] is a microscopic model that is developed to describe nucleon-induced reactions. It assumes the nucleon-nucleon collision as a cascade process involving a succession of binary collisions, and particles move along straight trajectories between collisions. The cascade process ceases to give way to the evaporation step when the remnant is fairly well equilibrated [45]. In the calculations, the ABLA evaporation model is included in the standard distribution of the INCL++ code. As displayed in Fig. 5, the general trend of the experimental data is satisfactorily reproduced by INCL++.

The measured results are further compared with the Particle and Heavy Ion Transport code System (PHITS) [46], which describes the nucleus-nucleus reactions by combining the JAERI quantum molecular dynamic model (JQMD) [47] and the Generalized Evaporation Model (GEM) [48]. The calculations are performed with both JQMD and JQMD-2.0 [34]. The JQMD-2.0 is modified from JQMD by considering the relativistic covariance of the Hamiltonian and revising the neutron-proton scattering cross section when scattering occurs near the nuclear surface. With these modifications, JQMD-2.0 can better simulate peripheral collisions. As shown in Fig. 5, the JQMD reproduces the general trend of experimental data well but underestimates the data, while JQMD-2.0 overestimates the data.

IV. SUMMARY

Systematic measurements of the elemental fragmentation cross sections of boron fragments from stable and neutron-rich $^{12-16}$C beams were performed at the ETF of the Institute of Modern Physics, Chinese Academy of Sciences. The incident beam energy was approximately 240 MeV/nucleon, and a carbon target was employed. The results show that the cross sections are dependent on the neutron-to-proton ratio of the carbon projectiles, that is, the cross sections increase evenly with increasing projectile neutron number. This trend can be qualitatively understood using the abrasion-ablation two-step model.

The experimental data were also compared with EPAX3, modified EPAX2, FRACS, NUCFRG2, INCL++, JQMD, and JQMD-2.0. All predictions made by these models agree reasonably well with the measured cross sections within a factor of 2. The general trend of the present data can be satisfactorily reproduced using INCL++ calculations. Furthermore, the predicted odd-even staggering feature by FRACS, JQMD-2.0, and the abrasion-ablation model is observed from ^{12}C to ^{14}C but not ^{14}C to ^{16}C in this experiment. The NUCFRG2 model predicts an incorrect trend compared to the data. Our current measurements can be used to benchmark and improve related models for light neutron-rich regions. In the future, more fragmentation data for neutron-rich nuclei in heavier regions are expected to be measured at the ETF of CSR; this can further serve to illustrate the effect of isospin on the fragmentation process and thus help to evaluate the validity of various predictions.

ACKNOWLEDGMENT

The authors thank the HIRFL accelerator staff for preparing the primary and secondary beams.

References

[1] I. Tanihata *et al*., Phys. Rev. Lett. **55**, 2676-2679 (1985)
[2] I. Tanihata, H. Savajols, and R. Kanungo, Prog. Part. Nucl. Phys. **68**, 215-313 (2013)
[3] T. Nakamura, H. Sakurai, and H. Watanabe, Prog. Part. Nucl. Phys. **97**, 53-122 (2017)
[4] A. Ozawa *et al*., Nucl. Phys. A **691**, 599-617 (2001)
[5] O. B. Tarasov *et al*., Phys. Rev. Lett. **102**, 142501 (2009)
[6] K. Kisamori *et al*., Phys. Rev. Lett. **116**, 052501 (2016)
[7] M. Stanoiu *et al*., Phys. Rev. C **69**, 034312 (2004)
[8] C.-W. Ma *et al*., Prog. Part. Nucl. Phys. **121**, 103911 (2021)
[9] D. Pérez-Loureiro *et al*., Phys. Lett. B **703**, 552-556 (2011)
[10] T. Kanai *et al*., Int. J. Radiat. Oncol. Biol. Phys. **44**, 201-210 (1999)
[11] M. Suzuki *et al*., Int. J. Radiat. Oncol. Biol. Phys. **48**, 241-250 (2000)
[12] M. Toppi *et al*., Phys. Rev. C **93**, 064601 (2016)
[13] T. Brohm and K.-H. Schmidt, Nucl. Phys. A **569**, 821-832 (1994)
[14] Y. Yariv and Z. Fraenkel, Phys. Rev. C **20**, 2227-2243 (1979)
[15] K. Sümmerer, Phys. Rev. C **86**, 014601 (2012)
[16] B. Mei, Phys. Rev. C **95**, 034608 (2017)
[17] J. Wilson *et al*., Nucl. Instrum. Methods Phys. Res. B **94**, 95-102 (1994)
[18] R. Thies *et al*., Phys. Rev. C **93**, 054601 (2016)
[19] T. Toshito *et al*., Phys. Rev. C **75**, 054606 (2007)
[20] W. R. Webber, J. C. Kish, and D. A. Schrier, Phys. Rev. C **41**, 547-565 (1990)
[21] H. Tsujii *et al*., J. Radiat. Res. **48**, A1-A13 (2007)
[22] U. Amaldi and G. Kraft, Rep. Prog. Phys. **68**, 1861-1882 (2005)
[23] M. Durante and K. Parodi, Front. Phys. **8**, 326 (2020)
[24] J. Xia *et al*., Nucl. Instrum. Methods Phys. Res. A **488**, 11-25 (2002)
[25] W. Zhan *et al*., Nucl. Phys. A **805**, 533c-540c (2008)
[26] X. Zhou *et al*., Nucl. Sci. Tech. **32**, 37 (2021)
[27] Y.-J. Wang *et al*., Nucl. Sci. Tech. **32**, 4 (2021)
[28] B.-H. Sun *et al*., Sci. Bull. **63**, 78-80 (2018)
[29] Y. Sun *et al*., Nucl. Instrum. Methods Phys. Res. A **927**, 390-395 (2019)
[30] W.-J. Lin *et al*., Chin. Phys. C **41**, 066001 (2017)
[31] K. Kimura *et al*., Nucl. Instrum. Methods Phys. Res. A **538**, 608-614 (2005)
[32] C. Zeitlin *et al*., Phys. Rev. C **76**, 014911 (2007)
[33] J. M. Kidd *et al*., Phys. Rev. C **37**, 2613-2623 (1988)

[34] T. Ogawa *et al*., Phys. Rev. C **92**, 024614 (2015)
[35] J.-J. Gaimard and K.-H. Schmidt, Nucl. Phys. A **531**, 709-745 (1991)
[36] R. Serber, Phys. Rev. **72**, 1114-1115 (1947)
[37] K. Sümmerer *et al*., Phys. Rev. C **42**, 2546-2561 (1990)
[38] O. Tarasov and D. Bazin, Nucl. Instrum. Methods Phys. Res. B **266**, 4657-4664 (2008)
[39] R. Kanungo *et al*., Phys. Rev. Lett. **117**, 102501 (2016)
[40] A. Leistenschneider *et al*., Phys. Rev. C **65**, 064607 (2002)
[41] K. Sümmerer and B. Blank, Phys. Rev. C **61**, 034607 (2000)
[42] X. Zhang, Nucl. Phys. A **915**, 59-69 (2013)
[43] J. W. Wilson, L. W. Townsend, and F. Badavi, Nucl. Instrum. Methods Phys. Res. B **18**, 225-231 (1986)
[44] J. Hirtz *et al*., Phys. Rev. C **101**, 014608 (2020)
[45] A. Boudard *et al*., Phys. Rev. C **87**, 014606 (2013)
[46] T. Sato *et al*., J. Nucl. Sci. Technol **55**, 684-690 (2018)
[47] K. Niita *et al*., Phys. Rev. C **52**, 2620-2635 (1995)
[48] S. Furihata, Nucl. Instrum. Methods Phys. Res. Sect. B **171**, 251-258 (2000)